ACS APPLIED MATERIALS & INTERFACES

Research Article

www.acsami.org

Solution-Processed Highly Conductive PEDOT:PSS/AgNW/GO Transparent Film for Efficient Organic-Si Hybrid Solar Cells

Qiaojing Xu, Tao Song,* Wei Cui, Yuqiang Liu, Weidong Xu, Shuit-Tong Lee, and Baoquan Sun*

Jiangsu Key Laboratory for Carbon-Based Functional Materials & Devices, Institute of Functional Nano & Soft Materials (FUNSOM), Soochow University, 199 Ren'ai Road, Suzhou 215123, P.R. China

Supporting Information

ABSTRACT: Hybrid solar cells based on n-Si/poly(3,4-ethylenedioxythiophene):poly(styrene- sulfonate) (PEDOT:PSS) heterojunction promise to be a low cost photovoltaic technology by using simple device structure and easy fabrication process. However, due to the low conductivity of PEDOT:PSS, a metal grid deposited by vacuum evaporation method is still required to enhance the charge collection efficiency, which complicates the device fabrication process. Here, a solution-processed graphene oxide (GO)-welded silver nanowires (AgNWs) transparent conductive electrode (TCE) was employed to replace the vacuum deposited metal grid. A unique "sandwich" structure was developed by embedding an AgNW network between PEDOT:PSS and GO with a figure-of-merit of $8.6 \times 10^{-3}\ \Omega^{-1}$, which was even higher than that of sputtered indium tin oxide electrode ($6.6 \times 10^{-3}\ \Omega^{-1}$). A champion power conversion efficiency of 13.3% was achieved, because of the decreased series resistance of the TCEs as well as the enhanced built-in potential (V_{bi}) in the hybrid solar cells. The TCEs were obtained by facile low-temperature solution process method, which was compatible with cost-effective mass production technology.

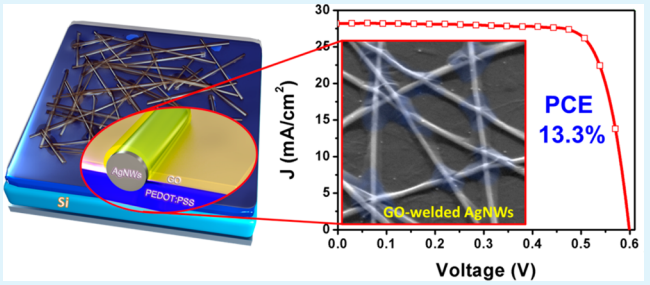

KEYWORDS: *silver nanowires, graphene oxide, solution-processed, transparent conductive electrode, hybrid silicon solar cell*

INTRODUCTION

Crystalline silicon solar cells stand for more than 90% of the photovoltaic (PV) market share, owing to the high power conversion efficiency (PCE) as well as the sufficient raw material supply. But the high cost of silicon solar cells is still the main obstacle for their large-scale applications because of the complex and energy-consuming fabrication processes as well as the high material costs.[1,2] Recently, organic−inorganic hybrid solar cells based on conductive conjugated polymers and crystalline silicon substrates attract wide research interests.[3−6] The hybrid solar cells can combine the advantages of both organic and inorganic counterparts. First, the crystalline silicon substrates ensure excellent light-harvesting properties. Second, the high-temperature dopant diffusion processes are avoided because the PV effect of the hybrid solar cells comes from the heterojunction formed by depositing organic layers on silicon substrates. Moreover, the facile low-cost solution techniques could be employed to process the organic materials in the hybrid devices. The conjugated polymer of poly(3,4-ethylenedioxythiophene):poly(styrenesulfonate) (PEDOT:PSS) is widely used as hole-transporting window in the hybrid solar cell because of its high conductivity and transparency.[7−12] However, extra electrodes, such as indium tin oxide (ITO) and metal grids, are usually required to further improve the lateral charge transport property of the PEDOT:PSS films in the hybrid devices.[13−15] Silver (Ag) grid electrodes (thickness of 200 nm) are commonly deposited on PEDOT:PSS layers by vacuum thermal evaporation methods through shadow masks. But the deposition process is time-consuming and costly. Meanwhile, a certain proportion of incident light will be either reflected or blocked by the thick Ag grids, leading to decreased light absorption of the solar cells. Therefore, a cost-effective and highly conductive transparent conductive electrode (TCE) under mild conditions is expected to enhance the performance of the hybrid solar cell.

Alternative solution-processed TCEs, such as carbon nanotubes (CNTs),[16,17] graphene,[18,19] and metal nanowires,[8,20−23] have been extensively investigated in recent years. The CNTs networks and graphene films exhibit a great flexibility and transparency, which could be used to fabricate PV devices. But sheet resistance (R_s) of the carbon-based TCEs is still inferior to conventional ITO electrodes.[24] The random network of silver nanowires (AgNWs) shows a promising high conductivity (~9.4 Ω/sq) and an excellent transmittance of over 90% in the visible light range.[25]

However, large surface roughness and poor charge transport across the junctions between adjacent AgNWs need to be further improved for PV applications. Generally, several postprocessing treatments, such as high-temperature thermal annealing,[20] mechanical pressing,[26] hydrogen chloride vapor

Received: November 15, 2014
Accepted: January 20, 2015
Published: January 20, 2015

DOI: 10.1021/am508006q
ACS Appl. Mater. Interfaces 2015, 7, 3272−3279

exposure,[27] plasmonic welding,[28] and joule heating welding,[29] are necessary to ensure high conductivity and strong adhesion of AgNW networks on substrates. Recently, composite TCEs were fabricated with AgNWs and other functional materials to overcome the drawbacks of the single-component AgNW electrodes.[30−34] Likewise, by assembling graphene oxide (GO) with AgNWs, the film R_s could be decreased because the AgNWs provided conductive paths for charge carrier to transport across the grain boundaries of GO.[35]

Herein, solution-processed GO was utilized as ultrathin overcoating layer to effectively weld AgNW junctions combined with PEDOT:PSS to improve film conductivity without sacrifice of light transparency. The as-fabricated AgNW/GO composite films were applied on top of PEDOT:PSS to replace the vacuum deposited metal grid electrodes in Si/PEDOT:PSS hybrid solar cells. The tightly welded AgNW networks were sandwiched between GO and PEDOT:PSS. Owing to the lower optical loss and the improved conductivity of the AgNW/GO films as well as the deepened work function (WF) of the PEDOT:PSS films induced by GO, a champion PCE of as high as 13.3% was achieved, which was even higher than that of the reference devices with conventional vacuum deposited Ag grid electrodes. Meanwhile, except for the vacuum deposited back contacts, the whole fabrication processes of the hybrid solar cells are based on fully solution-processed methods at room temperature, which is compatible with the mass-production technologies. As a result, the PEDOT:PSS/AgNW/GO composite TCEs could be potentially used to further reduce the fabrication cost of the organic−inorganic hybrid solar cells.

RESULTS AND DISCUSSION

In the hybrid n-Si/PEDOT:PSS solar cells, PV effect was generated from the heterojunction at the interface between the organic layers and the inorganic substrates. The crystalline n-type silicon substrates harvest the incident light and convert the photons into charge carriers. The light-induced holes and electrons are separated and driven to the PEDOT:PSS layer and the Al back electrode, respectively. The AgNW/GO films were coated on the PEDOT:PSS layers to improve the lateral charge transport property of holes in the TCEs.

To investigate the surface topography, transmittance, and conductivity of the composite TCEs, we fabricated PEDOT:PSS/AgNW/GO sandwiched triple layers on either glass substrates or silicon wafers, following the same processing condition in the device fabrication process.

The morphology of AgNW networks prepared with 2.5 mg/mL AgNW suspension with and without GO coverage was characterized by scanning electron microscopy (SEM) and atomic force microscope (AFM), as shown in Figure 1. The SEM image demonstrates that a randomly cross-linked AgNW network was built on silicon surface with a very low coverage ratio (about 10−15%) permitting a high light transmittance. After the GO thin film was deposited, the distribution of AgNWs remained same, and the whole AgNW network was encapsulated between GO and PEDOT:PSS. Especially, the cross junctions of AgNWs were welded tightly by GO, bridging the charge transport across adjacent AgNWs and lowering R_s of the AgNW networks. Surface roughness of the composite TCEs was further probed by AFM, as illustrated in Figure 1c, d. According to the AFM image, it was found that the surface morphology was smoothed with GO coating. Steep spikes and valleys in Figure 1c are due to the loose stacking of AgNWs, indicating that electrical contacts among the overlapping

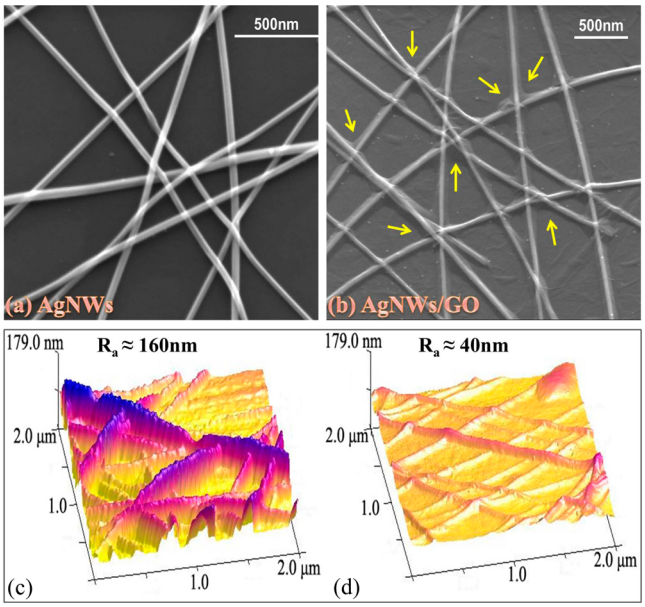

Figure 1. SEM images of as-fabricated pristine AgNW networks (a) before and (b) after GO coverage. Junctions in AgNW networks were effectively welded by the GO overcoating layer as indicated by the yellow arrows. Three-dimensional AFM images of the PEDOT:PSS/AgNW composite TCEs (c) before and (d) after the GO coverage. Surface roughness of AgNWs was reduced from 160 to 40 nm by the GO overcoating layer.

AgNWs could be further enhanced by making the network more compact. The root-mean-square (RMS) roughness dramatically decreased from 160 nm of the pristine AgNW network to 40 nm of the GO-covered AgNW one. The R_s also decreased from 66.1 to 23.1 Ω/sq. We believe that the charge transport enhancement of the composite film was ascribed to the following three points. First, electrical contact quality in the AgNW network was improved since the average spacing between the overlapping AgNWs was decreased after the GO coating. Second, contacting area between PEDOT:PSS and AgNWs was enlarged because of the smoothed morphology of the AgNW network. Third, the charge carriers could shuttle among AgNWs through GO, which wrapped on the AgNW junctions. For the AgNW film without GO coatings, connections between adjacent AgNWs were primarily driven by gravity force and van der Waals one.[33] The bonding strength was weak, which resulted in loose connections between AgNWs. After GO solution was spin-coated onto the AgNW network, the interconnection between AgNWs was greatly improved. There are plenty of oxygen-containing functional groups on GO nanosheet surface, including hydroxyl groups, carboxyl groups, and epoxide groups.[36,37] They are eligible to strongly bonding with AgNWs and underneath PEDOT:PSS caused by hydrophilic electrostatic interactions. The AgNW network could be firmly encapsulated between GO and PEDOT:PSS by the strong adhesion force. At the same time, the AgNW network could be pressed more tightly by the capillary forces during solvent evaporation process of GO solution, as inferred from Figure 1b. The junctions between AgNWs can be fused together compactly by the GO overcoating layer. Additionally, optical loss due to the ultrathin GO layer on the AgNW network is negligible (see Figure S2 in the Supporting Information), which is critical to achieving a high-performance solar cell. It is worth mentioning that there

DOI: 10.1021/am508006q
ACS Appl. Mater. Interfaces 2015, 7, 3272−3279

may be other materials with oxygen-containing functional groups that potentially exhibit similar effects as GO. An investigation into this mechanism in a subsequent study would further enhance the AgNW mesh conductivity.

R_s and film transparency of the as-prepared composite TCEs were measured accordingly, as shown in Figure 2 and Figure S2, and summarized in Table S1 in the Supporting Information. The films fabricated from various concentrations of AgNWs in the range of 1−5 mg/mL were investigated. Uniform AgNW networks could be formed on annealed PEDOT:PSS films by spin coating method. Conductive AgNW networks provide additional charge transport pathways, significantly reducing the R_s of the PEDOT:PSS films, as shown in Figure 2a. An obvious gradient of R_s variations in the AgNW/PEDOT:PSS composite films coated with different concentrations of AgNW suspensions was observed. R_s gradually increased with a decrease in the AgNW concentrations, until it was diluted to 1 mg/mL, in which case the distribution of AgNWs on PEDOT:PSS films was too sparse to form an effective charge transport path. After subsequent coating of GO layers, the AgNW networks were well-embedded between PEDOT:PSS and GO overcoating layers, with the internanowire junctions fused tightly together by the GO nanosheets. As a result, R_s of the PEDOT:PSS/AgNW/GO TCE was further reduced compared with that of the PEDOT:PSS/AgNW one. The dropping tendency of R_s with increasing AgNW concentration is as similar as that of the composite TCEs without GO layers. An R_s as low as 13.3 Ω/sq was achieved, which is comparable with ∼10 Ω/sq of commercial ITO glass.[20] For film fabricated from 1 mg/mL AgNW suspension with or without GO, R_s roughly remains the same, indicating that the conductivity improvement of PEDOT:PSS films mainly comes from the percolated AgNW networks.

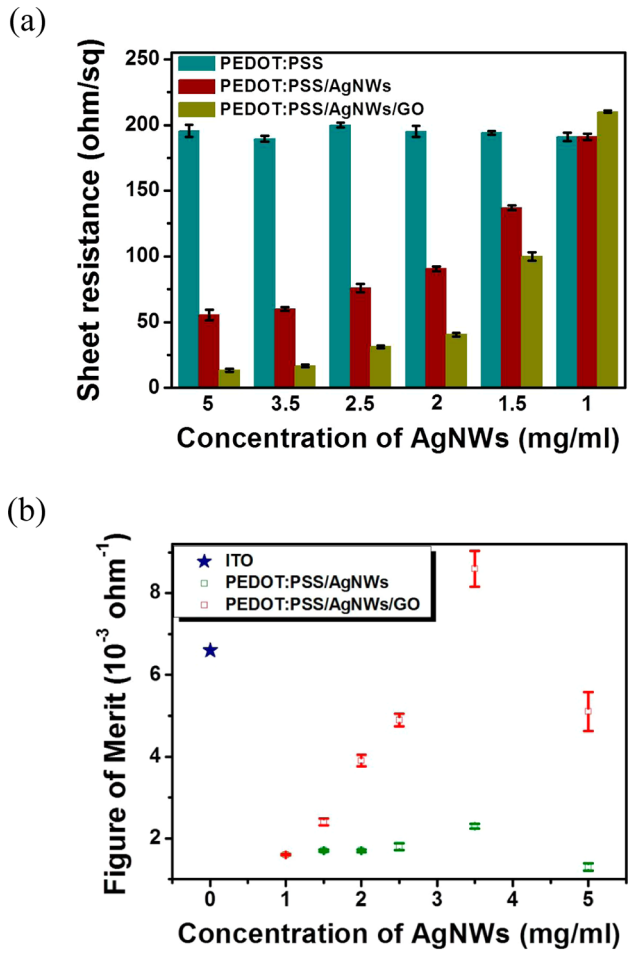

Figure 2. Electrical and optical characteristics of the TCEs. (a) Histograms of R_s of PEDOT:PSS, PEDOT:PSS/AgNW and PEDOT:PSS/AgNW/GO films. The statistics of R_s proposed in each group is obtained from five measurements in different regions of the corresponding films. (b) Figure of merit values of PEDOT:PSS/AgNWs with or without GO as a function of AgNW suspension concentration.

To further verify the key role of GO for the conductivity improvement of AgNWs, only the solvent of GO (mixed solvent of H_2O and isopropanol) was spin-coated onto AgNW mesh to measure conductivity change before and after solvent evaporation. The corresponding measured R_s values are summarized in Table S4 and plotted in Figure S3a in the Supporting Information. R_s shows slightly drop after solvent treatment, indicating that the AgNW network would be bonded more tightly not only by the capillary forces from solvent evaporation but also the hydrophilic electrostatic interactions between GO and underneath PEDOT:PSS. AgNW network can be fused more compactly by the interaction.

The transmittance spectra of pristine PEDOT:PSS film, PEDOT:PSS/AgNW and PEDOT:PSS/AgNW/GO composite films with various AgNW concentrations are shown in Figure S2 in the Supporting Information. The transmittance decreases with an increase in AgNW concentration, along with a drop at short wavelengths due to absorption of AgNWs by surface plasmons.[38] The corresponding transmittance at 550 nm is gradually reduced from 93.4% (1 mg/mL) to 82.8% (5 mg/mL). It is worth noting that in the hybrid PV devices, the trade-off between conductivity and transmittance of the PEDOT:PSS/AgNW/GO TCEs needs to be optimized by tuning AgNW concentration to balance light absorption and charge transport.

For in-depth analysis of the PEDOT:PSS/AgNW/GO composite TCEs, figure-of-merit (Φ_{TC}) was used to evaluate TCE quality, as defined by Haacke[39]

$$\Phi_{TC} = \frac{T_w^{10}}{R_s} \quad (1)$$

where T_w is the weighted-average transmittance over the range 350−1100 nm weighted by the current density of AM1.5G solar spectrum. By assuming all of the transmission light is absorbed by silicon, it can be obtained according to the following equation[8]

$$T_w = \frac{\int_{350nm}^{1100nm} T(\lambda) I_{AM1.5G}(\lambda) d\lambda}{\int_{350nm}^{1100nm} I_{AM1.5G}(\lambda) d\lambda} \quad (2)$$

in which $I_{AM1.5G}(\lambda)$ and $T(\lambda)$ represent the photon flux density of AM1.5G solar spectrum and the light transmittance at a certain incident wavelength λ, respectively. The as-integrated T_w of PEDOT:PSS/AgNW (3.5 mg/mL)/GO TCE (82.3%) is comparable with that of PEDOT:PSS/Ag grids (83.7%), as shown in Figure S3 in the Supporting Information. The calculated Φ_{TC} values were plotted as a function of the concentration of AgNW suspension, as shown in Figure 2b. GO addition onto the PEDOT:PSS/AgNW films can boost Φ_{TC} value remarkably. The maximum Φ_{TC} value is 8.6×10^{-3} Ω^{-1}

DOI: 10.1021/am508006q
ACS Appl. Mater. Interfaces 2015, 7, 3272−3279

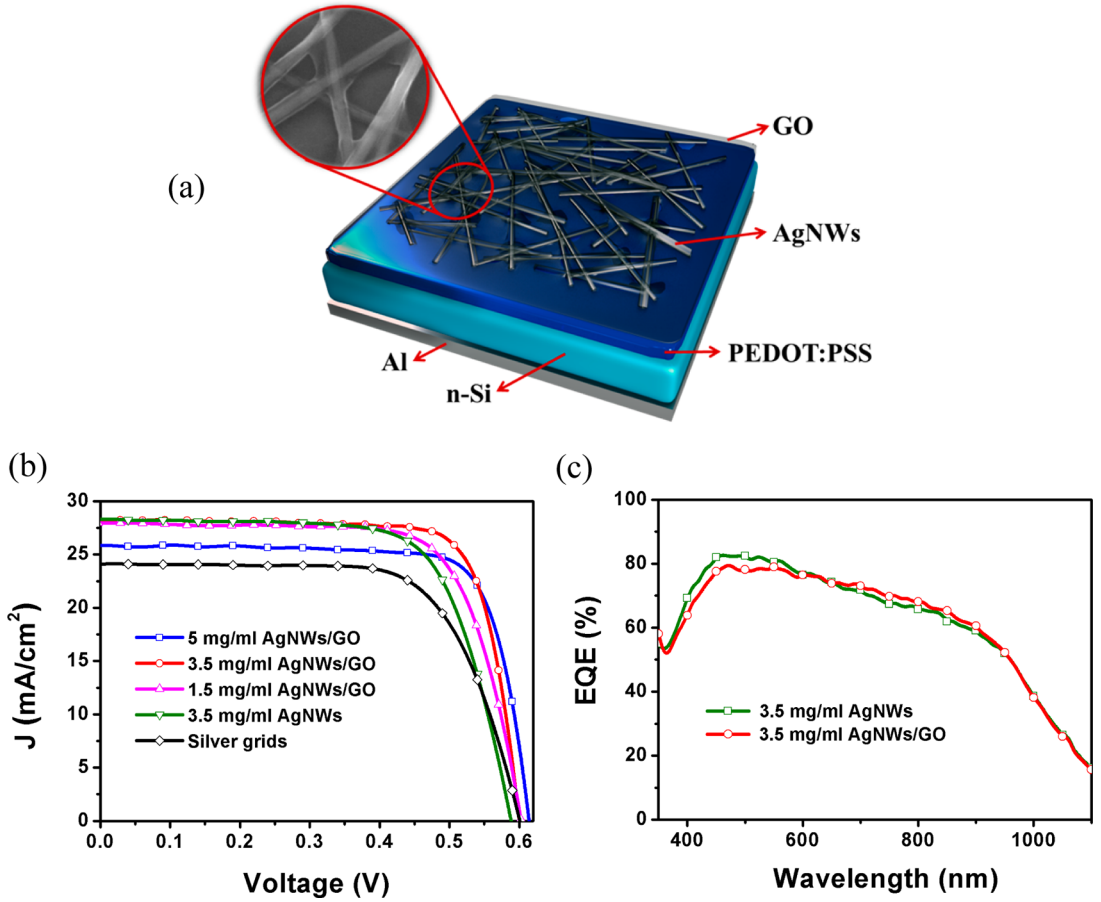

Figure 3. (a) Schematic diagram of the Si/PEDOT:PSS hybrid solar cells based on the PEDOT:PSS/AgNW/GO composite TCEs. (b) Current density versus voltage characteristics of the hybrid solar cells based on AgNW/GO composite TCEs with AgNW concentrations of 5, 3.5, and 1.5 mg/mL, silver grids electrode, and pristine AgNW TCE with a concentration of 3.5 mg/mL, respectively. (c) EQE spectra of the hybrid solar cells based on the PEDOT:PSS/AgNW and PEDOT:PSS/AgNW/GO TCEs with 3.5 mg/mL AgNW.

Table 1. Electrical Output Characteristics of Si/PEDOT:PSS Hybrid Solar Cells Based on the AgNW/GO Composite Electrodes

concentration of AgNWs[a](mg/mL)	J_{sc}[b] (mA/cm²)	V_{oc}[b] (V)	FF[b](%)	PCE[b](%)	series resistance (Ω cm²)
5	**25.4**	**0.610**	**78.6**	**12.2**	2.26
	25.4 ± 0.1	0.610 ± 0.002	78.6 ± 0.3	12.2 ± 0.0	
3.5	**28.4**	**0.601**	**78.4**	**13.3**	1.79
	28.1 ± 0.2	0.598 ± 0.003	78.7 ± 0.3	13.2 ± 0.1	
2.5	**27.5**	**0.610**	**73.7**	**12.4**	2.39
	27.4 ± 0.2	0.609 ± 0.002	73.8 ± 0.2	12.3 ± 0.1	
2	**27.6**	**0.602**	**72.9**	**12.1**	2.41
	27.6 ± 0.3	0.602 ± 0.001	72.5 ± 0.8	12.0 ± 0.1	
1.5	**28.0**	**0.602**	**72.8**	**12.3**	2.45
	28.1 ± 0.3	0.602 ± 0.002	71.9 ± 0.9	12.2 ± 0.1	

[a]Data and statistics based on five cells of each concentration. [b]Numbers in bold are the maximum record values.

for the GO-coated PEDOT:PSS/AgNW film, which is even higher than that of sputtered ITO electrode (6.6×10^{-3} Ω^{-1}).[8]

To directly investigate the electrical properties of PEDOT:PSS/AgNW/GO TCE for solar cell application, we performed an electrical simulation relevant to the light transmittance via the relation as follows

$$\langle J_{sc} \rangle = q \int_{350nm}^{1100nm} I_{1.5}(\lambda) \mathrm{EQE}(\lambda) T(\lambda) d\lambda \quad (3)$$

where $\langle J_{sc} \rangle$ denotes the simulated current density. $I_{1.5}(\lambda)$ and $T(\lambda)$ have the same meaning with the corresponding ones in eq 2, respectively, and q is the elementary charge. EQE(λ) is the external quantum efficiency of solar cell, and here it is assumed to be equal to 100%. The integrated $\langle J_{sc} \rangle$ are 32.7 and 31.4 mA/cm² for PEDOT:PSS/Ag grids and PEDOT:PSS/AgNW (3.5 mg/mL)/GO TCEs, respectively, inferring comparable electrical properties of these two systems (Table S4 in the Supporting Information).

The schematic device structure of the organic−inorganic hybrid solar cells based on the PEDOT:PSS/AgNW/GO composite TCEs is depicted in Figure 3a. Different top electrodes, including thermal evaporated silver grids and

DOI: 10.1021/am508006q
ACS Appl. Mater. Interfaces 2015, 7, 3272−3279

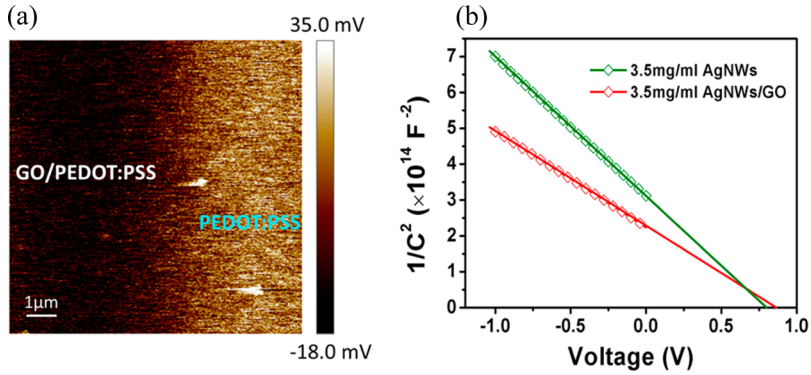

Figure 4. (a) Surface potential profile of the PEDOT:PSS film with (left part) and without (right part) GO. (b) $1/C^2-V$ plots of the hybrid solar cells based on AgNW and AgNW/GO TCEs with 3.5 mg/mL AgNWs.

solution processed pristine AgNW networks, were also fabricated for comparison.

The hybrid solar cells with different kinds of top anodes were measured under simulated AM1.5 solar illumination at 100 mW/cm^2. Figure 3b illustrates the current density−voltage ($J-V$) characteristics of the hybrid solar cells based on AgNW/GO composite TCEs with AgNW concentrations of 5, 3.5, and 1.5 mg/mL; silver grid electrode;and pristine AgNW TCE with a concentration of 3.5 mg/mL. The short-circuit current density (J_{sc}), the open-circuit voltage (V_{oc}), the fill factor (FF), and the PCE of solar cells with different top anodes are summarized in Table 1 and Table S2 in the Supporting Information. The devices based on PEDOT:PSS/AgNW/GO TCEs show higher PCE than those based on either conventional Ag grids or PEDOT:PSS/AgNW TCEs without GO. With the GO layer, the PCE of the hybrid devices is enhanced from ∼11 to ∼12% on average. In particular, the FF is significantly improved by integration of GO because of reduced series resistance of the devices (Table 1 and Table S2 in the Supporting Information). Series resistance was extracted from slope of $J-V$ curves at J = 0.[40] Series resistance of the devices with PEDOT:PSS/AgNW/GO TCEs is much lower than that of the device without GO and the Ag grids device. Series resistance of solar cells is influenced by the lateral R_s as well as the contact resistance.[41] Lateral resistance of PEDOT:PSS films was reduced by the percolated AgNW networks. Meanwhile, contact resistance of the "sandwich" structure of PEDOT:PSS/AgNW/GO is low because of the strong electrostatic adhesion between hydrophilic PEDOT:PSS and GO.

By analyzing the device performance, we found that GO tended to take a more prominent role in the sparse distributed AgNW network than the densely packed one. Specifically, for the GO-covered device fabricated from 1.5 mg/mL AgNWs, the FF and the PCE were improved by 12.2 and 11.8%, respectively. While for the GO-covered device with a higher AgNW concentration of 5 mg/mL, the corresponding FF and the PCE were slightly increased by 5.4 and 3.4%, respectively. This phenomenon can be explained as follows: due to the loose morphology of the AgNW mesh, the sparse AgNW network cannot provide enough conducting paths to deliver charge carriers generated by light; it could be readily compensated by increasing the amount of contacting junctions and decreasing the junction resistance in AgNW network by the GO sheets coating. For the dense AgNW network, the R_s is already very low and the space for further improvements by the GO coverage is rather limited. As a result of a balance between light absorption and charge carrier collection, a remarkable PCE of 13.3% (with a J_{sc} of 28.4 mA/cm^2, a V_{oc} of 0.601 V, and a FF of 78.4%) was achieved employing the PEDOT:PSS/AgNW/GO composite TCEs with a AgNW suspension concentration of 3.5 mg/mL. It is worth noting that this result is also consistent with the maximum Φ_{TC} value of the PEDOT:PSS/AgNW/GO composite TCEs fabricated from 3.5 mg/mL AgNW concentration. The reference device based on the PEDOT:PSS/AgNW TCE with the same AgNW concentration exhibited a lower PCE of 11.6% (with a J_{sc} of 28.3 mA/cm^2, a V_{oc} of 0.579 V and a FF of 70.9%), which may be partially caused by the large roughness of the pristine AgNW mesh. The performance of the reference devices was consistent with the previous results where nanostructured silicon substrates were employed as photoactive layers and PEDOT:PSS/AgNWs acted as TCEs.[8] We believe that the higher efficiency of the hybrid solar cell based on PEDOT:PSS/AgNW/GO composite TCE can be attributed to the more efficient charge carrier collection and transfer, wherein the AgNW networks were effectively welded by GO nanosheets.

Though electrical conductivity has been improved using composite electrode with and without GO coverage, similar J_{sc} was obtained for those two types of devices. According to the EQE spectra of hybrid solar cells as shown in Figure 3c, the calculated J_{sc} was 27.8 and 27.7 mA/cm^2 for the devices with PEDOT:PSS/AgNW electrodes and PEDOT:PSS/AgNW/GO composite electrodes, respectively. The integrated J_{sc} values are in good accordance with those extracted from the $J-V$ characteristics. EQE spectra are closely correlated with both optical and electrical characteristics of the solar cells, such as light trapping and electrode conductivity, as well as charge separation and transfer in the devices. As shown in Figure S2d in the Supporting Information, reflectance is almost the same for the PEDOT:PSS/AgNW films with or without GO, indicating that light reflection is not the main reason for PV performance difference. On the other hand, we compared light transmittance of the PEDOT:PSS/AgNW films and the PEDOT:PSS/AgNW/GO ones, as shown in Figure S2c in the Supporting Information. This analysis confirms that for the devices with PEDOT:PSS/AgNW/GO composite TCEs, the slight decrease of EQE at the wavelengths shorter than 600 nm is caused by the light absorption of GO. The improvement at longer wavelengths is ascribed to enhanced charge transport and collection in the GO-covered TCEs. Finally, almost the same photocurrents are achieved in the both cases.

In addition, the V_{oc} of the hybrid solar cells with PEDOT:PSS/AgNW electrodes is slightly improved with GO coating. We speculated that PEDOT:PSS WF was related with

DOI: 10.1021/am508006q
ACS Appl. Mater. Interfaces 2015, 7, 3272−3279

the interaction between PEDOT:PSS and GO. Built-in potential (V_{bi}) of the Si/PEDOT:PSS heterojunction is strongly dependent on WF of TCEs.[42] As previously described, within the sandwiched structure, GO could penetrate through the voids of AgNW networks to contact directly with the PEDOT:PSS underlayer driven by their strong electrostatic adhesion force. From the SEM images (Figure 1), the shadow ratios of AgNW network were only about 10−15%, a relatively small proportion, which indicated that the majority of charge carriers were separated among the region formed by PEDOT:PSS and GO layer, then effectively collected by AgNWs. To verify the assumption, we used the scanning Kelvin probe microscope (SKPM) measurements to probe the surface potential of the PEDOT:PSS/GO films, as shown in Figure 4a. A very small amount of GO solution was dropped onto the PEDOT:PSS film to form a clear boundary for SKPM measurements. WF can be estimated via the equation[43]

$$\mathrm{WF} = \Phi_{tip} - eV_{CPD} \quad (4)$$

in which Φ_{tip} is WF of the conductive tip, V_{CPD} is contact potential difference between sample and the tip, and e is the elementary charge. It was observed that the V_{CPD} of GO/PEDOT:PSS was approximately 40 mV more negative than that of PEDOT:PSS, indicating that WF was deepened with the GO coating. Higher WF resulted in larger V_{bi}, which interpreted the improved V_{oc} in the devices with GO.

To further confirm V_{bi} enhancement by the GO overcoating layers in the hybrid solar cells, capacitance versus voltage ($C-V$) characteristics of the devices based on PEDOT:PSS/AgNW and PEDOT:PSS/AgNW/GO electrodes were investigated, as shown in Figure 4b. The $1/C^2$ value scales linearly with the bias voltage (V) according to the Schottky Mott relation[44]

$$1/C^2 = 2(V + V_{bi})/eN_D\varepsilon_s\varepsilon_0 \quad (5)$$

where N_D is the doping level of the semiconductor and ε_0 and ε_s are the permittivity of vacuum and the semiconductor, respectively. V_{bi} can be extracted from the extrapolation of $1/C^2$ to the horizontal axis. The V_{bi} of the device with PEDOT:PSS/AgNW/GO composite electrode is 0.84 V, which is about 40 mV larger than 0.80 V of the reference device without GO coating. The V_{bi} enhancement derived from the $C-V$ measurements is consistent with the result obtained from the SKPM measurement. The enlarged V_{bi} allows for a wider depletion region, which is favorable for better separation of photon-generated carriers, resulting in the improvement of the V_{oc}. Moreover, the enhanced V_{bi} is beneficial for the charge transfer and collection, thus contributing to the increase of the FF.

CONCLUSION

In summary, GO nanosheets were employed as adhesive materials to effectively weld the AgNW junctions combined with PEDOT:PSS in order to decrease the R_s of percolated AgNW/PEDOT:PSS networks. By sequentially spin-coating the AgNW suspension and the GO solution on the PEDOT:PSS layers, composite TCEs with a unique sandwiched structure were fabricated. A low R_s of 13.3 Ω/sq was obtained in the composite TCE with a transmittance of 82.8%, which is comparable with that of commercial ITO glass. The flat PEDOT:PSS/AgNW/GO TCEs were employed in organic−inorganic solar cells based on crystalline silicon substrates to replace the traditional vacuum deposited Ag grid electrodes. By optimizing light transmittance and R_s of the composite TCEs, a high PCE of 13.3% was achieved. The integration of GO improves the FF and the V_{oc} by reducing the series resistance and enhancing the V_{bi} of hybrid solar cells. Furthermore, the composite TCEs were fabricated by full solution-processed method under mild processing temperature. This facile technique to prepare highly transparent and conductive electrodes may contribute to the development of cost-effective organic−inorganic hybrid silicon solar cells.

EXPERIMENTAL SECTION

PEDOT:PSS/AgNW/GO Composite Electrode Fabrication. AgNWs were purchased from Kechuang Advanced Materials Co., Ltd. (Hangzhou, Zhejiang, China) with an average diameter of 25−35 nm and length of 10−20 μm. AgNW suspension (10 mg/mL in ethanol as purchased) was diluted with isopropyl alcohol (IPA) to various required concentrations and shaken for at least 5 min before using. GO was synthesized and purified using a modified Hummers method.[36] The original GO aqueous solution was diluted to 1 mg/mL with IPA, and ultrasonicated for 30 min at room temperature. Highly conductive PEDOT:PSS (Heraeus PH 1000) solution mixed with 5 wt % dimethyl sulfoxide (DMSO) and 1 wt % Triton (Sigma-Aldrich) was spin-coated onto clean glasses or silicon substrates under a rotation speed of 3600 r/min, followed by a subsequent annealing process at 125 °C in nitrogen atmosphere for 15 min to remove the solvent and enhance the $\pi-\pi$ stacking of the conjugated polymer chains.[45] After cooling to room temperature, the AgNW suspension with various concentrations and the GO solution (1 mg/mL) was sequentially spin-coated layer by layer on the PEDOT:PSS covered substrates. No further post-treatment was required.

Hybrid Device Fabrication. Clean n-type monocrystalline silicon (100) wafers (290 ± 10 μm, single-side polished) with a resistivity of 0.05−0.1 Ω cm were dipped in an aqueous solution of 5 M hydrofluoric acid (HF) to obtain clean oxide-free silicon surfaces. The fabrication of top anode electrodes was followed by the same steps as described in the PEDOT:PSS/AgNW/GO composite electrodes fabrication section. For the preparation of reference devices with conventional Ag grids as anodes, the Ag grids defined by a shadow mask was deposited onto the PEDOT:PSS-coated silicon substrates by a thermal evaporator (NANO 36, Kurt J. Lesker). Finally, a 200 nm thick Al layer was thermally evaporated onto the rear surface of the silicon substrates.

Optical and Electrical Characterizations. Transmittance and reflectance spectra were measured by employing an integrating sphere (PerkinElmer Lambda 700). The R_s measurement was carried out by a standard four-point probe system (ST-2258A, Suzhou Jingge Electronic Co., LTD). The R_s proposed here is the mean value averaged over five measurements. The SEM images were obtained by a FEI Quanta 200 FEG. The $J-V$ characteristics were tested using a Newport solar simulator to generate simulated air mass (AM) 1.5 solar spectrum irradiation source at 100 mW/cm^2. The EQE was measured by a Keithley source meter under different wavelength light generated by a Newport monochromator 74125. The morphologies of the PEDOT:PSS/AgNW/GO and surface potentials of the PEDOT:PSS/GO film were obtained by AFM and SKPM (Veeco, Multimode V), respectively. The $C-V$ measurement was performed with a Keithley 4200 semiconductor characterization system at a frequency of 1 kHz.

ASSOCIATED CONTENT

Supporting Information

Topography images of various electrodes, transmittance and reflectance of different films, histograms of sheet resistance of PEDOT:PSS/AgNW electrodes before and after solvent of GO treatment and weighted transmittance of various electrodes versus the concentration of AgNWs. Data tables for optical and electrical characteristics of different electrodes, electrical output characteristics of the reference devices, and electrical simulation

DOI: 10.1021/am508006q
ACS Appl. Mater. Interfaces 2015, 7, 3272−3279

data for different electrodes. This material is available free of charge via the Internet at http://pubs.acs.org/.

AUTHOR INFORMATION

Corresponding Authors

*E-mail: tsong@suda.edu.cn. Tel: 0086-512-65880951.
*E-mail: bqsun@suda.edu.cn.

Notes

The authors declare no competing financial interest.

ACKNOWLEDGMENTS

This work was supported by the National Basic Research Program of China (973 Program) (2012CB932402), the National Natural Science Foundation of China (91333208, 61176057, 91123005), the Priority Academic Program Development of Jiangsu Higher Education Institutions, Natural Science Foundation of Jiangsu Province of China (BK20130310), Collaborative Innovation Center of Suzhou Nano Science and Technology.

REFERENCES

(1) Little, R. G.; Nowlan, M. J. Crystalline Silicon Photovoltaics: the Hurdle for Thin Films. *Prog. Photovolt.: Res. Appl.* **1997**, *5*, 309−315.
(2) Fthenakis, V. M.; Kim, H. C. Photovoltaics: Life-Cycle Analyses. *Sol. Energy* **2011**, *85*, 1609−1628.
(3) Chen, T. G.; Huang, B. Y.; Chen, E. C.; Yu, P.; Meng, H. F. Micro-Textured Conductive Polymer/Silicon Heterojunction Photovoltaic Devices with High Efficiency. *Appl. Phys. Lett.* **2012**, *101*, 033301.
(4) Avasthi, S.; Lee, S.; Loo, Y. L.; Sturm, J. C. Role of Majority and Minority Carrier Barriers Silicon/Organic Hybrid Heterojunction Solar Cells. *Adv. Mater.* **2011**, *23*, 5762−5766.
(5) He, L.; Jiang, C.; Wang, H.; Lai, D. Rusli. High Efficiency Planar Si/Organic Heterojunction Hybrid Solar Cells. *Appl. Phys. Lett.* **2012**, *100*, 073503.
(6) Zhang, F.; Sun, B.; Song, T.; Zhu, X.; Lee, S. Air Stable, Efficient Hybrid Photovoltaic Devices Based on Poly(3-hexylthiophene) and Silicon Nanostructures. *Chem. Mater.* **2011**, *23*, 2084−2090.
(7) Shiu, S.-C.; Chao, J.-J.; Hung, S.-C.; Yeh, C.-L.; Lin, C.-F. Morphology Dependence of Silicon Nanowire/Poly(3,4-ethylenedioxythiophene):Poly(styrenesulfonate) Heterojunction Solar Cells. *Chem. Mater.* **2010**, *22*, 3108−3113.
(8) Chen, T. G.; Huang, B. Y.; Liu, H. W.; Huang, Y. Y.; Pan, H. T.; Meng, H. F.; Yu, P. Flexible Silver Nanowire Meshes for High-efficiency Microtextured Organic-Silicon Hybrid Photovoltaics. *ACS Appl. Mater. Interfaces* **2012**, *4*, 6857−6864.
(9) Liu, Q.; Ono, M.; Tang, Z.; Ishikawa, R.; Ueno, K.; Shirai, H. Highly Efficient Crystalline Silicon/Zonyl Fluorosurfactant-Treated Organic Heterojunction Solar Cells. *Appl. Phys. Lett.* **2012**, *100*, 183901.
(10) Jeong, S.; Garnett, E. C.; Wang, S.; Yu, Z.; Fan, S.; Brongersma, M. L.; McGehee, M. D.; Cui, Y. Hybrid Silicon Nanocone-Polymer Solar Cells. *Nano Lett.* **2012**, *12*, 2971−2976.
(11) Yu, P.; Tsai, C.-Y.; Chang, J.-K.; Lai, C.-C.; Chen, P.-H.; Lai, Y.-C.; Tsai, P.-T.; Li, M.-C.; Pan, H.-T.; Huang, Y.-Y.; Wu, C.-I.; Chueh, Y.-L.; Chen, S.-W.; Du, C.-H.; Horng, S.-F.; Meng, H.-F. 13% Efficiency Hybrid Organic/Silicon-Nanowire Heterojunction Solar Cell via Interface Engineering. *ACS Nano* **2013**, *7*, 10780−10787.
(12) Liu, R.; Lee, S. T.; Sun, B. 13.8% Efficiency Hybrid Si/Organic Heterojunction Solar Cells with MoO_3 Film as Antireflection and Inversion Induced Layer. *Adv. Mater.* **2014**, *26*, 6007−6012.
(13) Liu, Z.; Wang, H.; Fung, M.-K.; Lee, C.-S.; Zhang, X.-H. Low-Cost Solar Cell Based on a Composite of Silicon Nanowires and a Highly Conductive Nonphotoactive Polymer. *Chem.—Eur. J.* **2013**, *19*, 17273−17276.
(14) Pudasaini, P. R.; Ruiz-Zepeda, F.; Sharma, M.; Elam, D.; Ponce, A.; Ayon, A. A. High Efficiency Hybrid Silicon Nanopillar-Polymer Solar Cells. *ACS Appl. Mater. Interfaces* **2013**, *5*, 9620−9627.
(15) Liu, Q.; Khatri, I.; Ishikawa, R.; Fujimori, A.; Ueno, K.; Manabe, K.; Nishino, H.; Shirai, H. Improved Photovoltaic Performance of Crystalline-Si/Organic Schottky Junction Solar Cells Using Ferroelectric Polymers. *Appl. Phys. Lett.* **2013**, *103*, 163503.
(16) Wu, Z.; Chen, Z.; Du, X.; Logan, J. M.; Sippel, J.; Nikolou, M.; Kamaras, K.; Reynolds, J. R.; Tanner, D. B.; Hebard, A. F.; Rinzler, A. G. Transparent, Conductive Carbon Nanotube Films. *Science* **2004**, *305*, 1273−1276.
(17) Ham, H. T.; Choi, Y. S.; Chee, M. G.; Cha, M. H.; Chung, I. J. PEDOT-PSS/Singlewall Carbon Nanotubes Composites. *Polym. Eng. Sci.* **2008**, *48*, 1−10.
(18) Matyba, P.; Yamaguchi, H.; Chhowalla, M.; Robinson, N. D.; Edman, L. Flexible and Metal-Free Light-Emitting Electrochemical Cells Based on Graphene and PEDOT-PSS as the Electrode Materials. *ACS Nano* **2010**, *5*, 574−580.
(19) Hong, W.; Xu, Y.; Lu, G.; Li, C.; Shi, G. Transparent Graphene/PEDOT−PSS Composite Films as Counter Electrodes of Dye-Sensitized Solar Cells. *Electrochem. Commun.* **2008**, *10*, 1555−1558.
(20) Lee, J.-Y.; Connor, S. T.; Cui, Y.; Peumans, P. Solution-Processed Metal Nanowire Mesh Transparent Electrodes. *Nano Lett.* **2008**, *8*, 689−692.
(21) Gaynor, W.; Lee, J.-Y.; Peumans, P. Fully Solution-Processed Inverted Polymer Solar Cells with Laminated Nanowire Electrodes. *ACS Nano* **2009**, *4*, 30−34.
(22) Krantz, J.; Stubhan, T.; Richter, M.; Spallek, S.; Litzov, I.; Matt, G. J.; Spiecker, E.; Brabec, C. J. Spray-Coated Silver Nanowires as Top Electrode Layer in Semitransparent P3HT:PCBM-Based Organic Solar Cell Devices. *Adv. Funct. Mater.* **2013**, *23*, 1711−1717.
(23) Rathmell, A. R.; Bergin, S. M.; Hua, Y. L.; Li, Z. Y.; Wiley, B. J. The Growth Mechanism of Copper Nanowires and Their Properties in Flexible, Transparent Conducting Films. *Adv. Mater.* **2010**, *22*, 3558−3563.
(24) Hecht, D. S.; Hu, L.; Irvin, G. Emerging Transparent Electrodes Based on Thin Films of Carbon Nanotubes, Graphene, and Metallic Nanostructures. *Adv. Mater.* **2011**, *23*, 1482−1513.
(25) Kim, A.; Won, Y.; Woo, K.; Kim, C.-H.; Moon, J. Highly Transparent Low Resistance ZnO/Ag Nanowire/ZnO Composite Electrode for Thin Film Solar Cells. *ACS Nano* **2013**, *7*, 1081−1091.
(26) Hu, L.; Kim, H. S.; Lee, J.-Y.; Peumans, P.; Cui, Y. Scalable Coating and Properties of Transparent, Flexible, Silver Nanowire Electrodes. *ACS Nano* **2010**, *4*, 2955−2963.
(27) Liu, C. H.; Yu, X. Silver Nanowire-Based Transparent, Flexible, and Conductive Thin Film. *Nanoscale Res. Lett.* **2011**, *6*, 75.
(28) Garnett, E. C.; Cai, W.; Cha, J. J.; Mahmood, F.; Connor, S. T.; Greyson Christoforo, M.; Cui, Y.; McGehee, M. D.; Brongersma, M. L. Self-Limited Plasmonic Welding of Silver Nanowire Junctions. *Nat. Mater.* **2012**, *11*, 241−249.
(29) Song, T.-B.; Chen, Y.; Chung, C.-H.; Yang, Y.; Bob, B.; Duan, H.-S.; Li, G.; Tu, K.-N.; Huang, Y.; Yang, Y. Nanoscale Joule Heating and Electromigration Enhanced Ripening of Silver Nanowire Contacts. *ACS Nano* **2014**, *8*, 2804−2811.
(30) Lee, J.; Lee, P.; Lee, H. B.; Hong, S.; Lee, I.; Yeo, J.; Lee, S. S.; Kim, T.-S.; Lee, D.; Ko, S. H. Room-Temperature Nanosoldering of a Very Long Metal Nanowire Network by Conducting-Polymer-Assisted Joining for a Flexible Touch-Panel Application. *Adv. Funct. Mater.* **2013**, *23*, 4171−4176.
(31) Gaynor, W.; Burkhard, G. F.; McGehee, M. D.; Peumans, P. Smooth Nanowire/Polymer Composite Transparent Electrodes. *Adv. Mater.* **2011**, *23*, 2905−2910.
(32) Xu, F.; Zhu, Y. Highly Conductive and Stretchable Silver Nanowire Conductors. *Adv. Mater.* **2012**, *24*, 5117−5122.
(33) Zhu, R.; Chung, C.-H.; Cha, K. C.; Yang, W.; Zheng, Y. B.; Zhou, H.; Song, T.-B.; Chen, C.-C.; Weiss, P. S.; Li, G.; Yang, Y. Fused Silver Nanowires with Metal Oxide Nanoparticles and Organic Polymers for Highly Transparent Conductors. *ACS Nano* **2011**, *5*, 9877−9882.

DOI: 10.1021/am508006q
ACS Appl. Mater. Interfaces 2015, 7, 3272−3279

(34) Lee, P.; Ham, J.; Lee, J.; Hong, S.; Han, S.; Suh, Y. D.; Lee, S. E.; Yeo, J.; Lee, S. S.; Lee, D.; Ko, S. H. Highly Stretchable or Transparent Conductor Fabrication by a Hierarchical Multiscale Hybrid Nanocomposite. *Adv. Funct. Mater.* **2014**, *24*, 5671−5678.
(35) Liang, J.; Li, L.; Tong, K.; Ren, Z.; Hu, W.; Niu, X.; Chen, Y.; Pei, Q. Silver Nanowire Percolation Network Soldered with Graphene Oxide at Room Temperature and Its Application for Fully Stretchable Polymer Light-Emitting Diodes. *ACS Nano* **2014**, *8*, 1590−1600.
(36) Hummers, W. S.; Offeman, R. E. Preparation of Graphitic Oxide. *J. Am. Chem. Soc.* **1958**, *80*, 1339−1339.
(37) Dikin, D. A.; Stankovich, S.; Zimney, E. J.; Piner, R. D.; Dommett, G. H.; Evmenenko, G.; Nguyen, S. T.; Ruoff, R. S. Preparation and Characterization of Graphene Oxide Paper. *Nature* **2007**, *448*, 457−60.
(38) Tao, A.; Kim, F.; Hess, C.; Goldberger, J.; He, R.; Sun, Y.; Xia, Y.; Yang, P. Langmuir−Blodgett Silver Nanowire Monolayers for Molecular Sensing Using Surface-Enhanced Raman Spectroscopy. *Nano Lett.* **2003**, *3*, 1229−1233.
(39) Haacke, G. New Figure of Merit for Transparent Conductors. *J. Appl. Phys.* **1976**, *47*, 4086.
(40) Pysch, D.; Mette, A.; Glunz, S. W. A Review and Comparison of Different Methods to Determine the Series Resistance of Solar Cells. *Sol. Energy Mater. Sol. Cells* **2007**, *91*, 1698−1706.
(41) Chung, C. H.; Song, T. B.; Bob, B.; Zhu, R.; Duan, H. S.; Yang, Y. Silver Nanowire Composite Window Layers for Fully Solution-Deposited Thin-film Photovoltaic Devices. *Adv. Mater.* **2012**, *24*, 5499−5504.
(42) Robertson, J. Band Alignment at Metal-Semiconductor and Metal-Oxide Interfaces. *Phys. Status Solidi A* **2010**, *207*, 261−269.
(43) Palermo, V.; Palma, M.; Samorì, P. Electronic Characterization of Organic Thin Films by Kelvin Probe Force Microscopy. *Adv. Mater.* **2006**, *18*, 145−164.
(44) Miao, X.; Tongay, S.; Petterson, M. K.; Berke, K.; Rinzler, A. G.; Appleton, B. R.; Hebard, A. F. High Efficiency Graphene Solar Cells by Chemical Doping. *Nano Lett.* **2012**, *12*, 2745−2750.
(45) Ho, P. K. All-Polymer Optoelectronic Devices. *Science* **1999**, *285*, 233−236.

DOI: 10.1021/am508006q
ACS Appl. Mater. Interfaces 2015, 7, 3272−3279